

RELIABLE VALIDATION BASED ON OPTICAL FLOW VISUALIZATION FOR CFD SIMULATIONS

JIANG Zonglin (姜宗林)[†]

(Key Laboratory of High-Temperature Gas Dynamics, Institute of Mechanics, Chinese Academy of Sciences,
Beijing 100080, China)

ABSTRACT: A reliable validation based on the optical flow visualization for numerical simulations of complex flowfields is addressed in this paper. Several test cases, including two-dimensional, axisymmetric and three-dimensional flowfields, were presented to demonstrate the effectiveness of the validation and gain credibility of numerical solutions of complex flowfields. In the validation, images of these flowfields were constructed from numerical results based on the principle of the optical flow visualization, and compared directly with experimental interferograms. Because both experimental and numerical results are of identical physical representation, the agreement between them can be evaluated effectively by examining flow structures as well as checking discrepancies in density. The study shows that the reliable validation can be achieved by using the direct comparison between numerical and experiment results without any loss of accuracy in either of them.

KEY WORDS: CFD validation, optical flow visualization, numerical simulation, numerical flow visualization

1 INTRODUCTION

The Computational Fluid Dynamics is now a promising technology since it is now possible to solve full Reynolds averaged Navier-Stokes equations on geometrically realistic three-dimensional problems with available supercomputers. This technology enables us to highlight physics in complex fluid flows that are difficult to be clearly visualized experimentally. However, it becomes increasingly important to validate numerical solutions before relying on them to explain any flow physics. The simulation of fluid flows involves two essential steps: (1) selecting a suitable mathematical model that describes the physical flow phenomena of interest and (2) developing numerical techniques to compute a solution of the mathematical model using digital computers. Both steps generally introduce approximations, therefore, the resulting numerical solutions may or may not represent the real fluid flows being considered. In addition, a good agreement between numerical and experimental results is necessary to confirm the physical phenomena observed from experiments, especially from the flow visualization of three-dimensional complex fluid flows. For example, the widely-used optical flow vi-

sualization produces only an integral view of three-dimensional flow fields by recording phase shifts or direction changes of the light ray passing through test sections due to density variations^[1~5]. Hence the phenomena observed from such images are not their direct images, therefore, not easily interpreted.

The study on verification and validation of numerical solutions has been carried out for decades, usually by comparing numerical results with exact solutions or experimental data at some measurement points in flowfields. However, most of the flowfields of interest nowadays are highly transient since many unsteady phenomena may be included, such as shock wave reflection, diffraction and interaction. The exact solutions for such fluid fields are not available, and usually, it is also not sufficient to compare numerical solutions with a limited set of point measurements from experiments. Only through a comparison with the data from the whole flowfield measured by non-intrusive techniques can the confidence in numerical solutions be established. From this point of view, a reliable validation has two aspects: one is a check on numerical values and the other is a check on characteristic flow structures. Such a validation is still a

challenging problem for simulating complex fluid flows in the Computational Fluid Dynamics.

The optical flow visualization has been applied to the validation of numerical solutions of CFD for many years. The most widely used method for two-dimensional flows is to display numerical results in the form of isopycnics, which can be compared with experimental infinite fringe interferograms (for example, Inoue et al.^[6]; Sasoh et al.^[7]; Sun et al.^[8] and Takayama and Jiang^[9]). The comparison in this way is quite informative since the interferometric fringe in two-dimensional flows gives an indication of density contours. However, the evaluation on the accuracy of numerical solutions is not easy because the corresponding position of numerical isopycnics within experimental fringes is difficult to locate accurately. Furthermore, in the case of axisymmetric or three-dimensional fluid flows, the evaluation becomes even more difficult because the fringes no longer correspond to the density contours, but represent averaged density variations along the light path. Using numerical results as initial values on boundaries to count fringes, Sun and Takayama^[8] reported a quantitative image analysis of infinite fringe interferograms to validate their numerical solutions. Useful comparison can be made with this technique but the accuracy varies with the method used in locating isopycnics within fringes. Finite-fringe interferograms can also be analyzed with image processing techniques as reported by Havener et al.^[3], Jiang et al.^[10] and Sharma et al.^[11]. More data is readily available by using those methods but a loss of accuracy in experimental data cannot be avoided. This is because each fringe is broadened to a certain width and the data is available only at the fringes. So, these methods require a linear interpolation between fringes to obtain the required data, which results in errors in highly non-linear flowfields. Fourier transform fringe analysis supplies more information with high accuracy but its application is limited when the heterodyning frequency of the finite fringe interferograms is low as discussed by Babinsky et al.^[2] and Bone^[12]. However, all of the above-mentioned methods are of limited use for three-dimensional unsteady flows. Tomographic reconstruction method can be used to obtain density information but it is experimentally intensive because one projection is insufficient to determine the density distribution and tens of density projections from different viewing directions have to be provided simultaneously (Parker^[13]; Morton et al.^[14]; Taketa et al.^[15]). With the above considerations, the strategy of creat-

ing numerical interferograms for a direct comparison with experiments was discussed for CFD validation by many authors (Babinsky et al.^[1]; Havener et al.^[3]; Jiang et al.^[16,17]; Tam et al.^[18]; Tamura and Fujii^[19]; Yates^[4]). From the number of fringes and their distributions, the accuracy of numerical solutions and the agreement on characteristic flow structures appearing in the results can be estimated. The algorithm for integrating density in axisymmetric flowfields was described by Havener et al.^[3] and three-dimensional density integration was performed by Yates^[4]. Recently, an efficient algorithm for the integration was developed by Jiang and Takayama^[5], which is much faster and can make the post-processing method more widely applicable.

In the paper, a reliable validation based on the optical flow visualization for numerical simulations of complex flowfields is addressed and several test cases of two-dimensional, axisymmetric and three-dimensional flowfields were presented to demonstrate the reliable validation through the direct comparison between numerical and experimental results. Various aspects of this validation are discussed in detail, especially for three dimensional cases, where a clear flow visualization is very difficult.

2 PRINCIPLE OF OPTICAL FLOW VISUALIZATION

Interferometry, schlieren and shadowgraph are three techniques widely used in the optical flow visualization. These optical techniques are based on the fact that as light passes through a flowfield its phase and direction are changed due to variations of the refractive index induced by non-uniform density in the flowfield. This makes it possible to analyze physical phenomena that are featured by density changes in the flowfields. Discussions on the above techniques appear in numerous text books and in the literature. A brief summary is given here for completeness.

In the case of ideal and non-reacting gases, the refractive index n is related to the density ρ by the Gladstone-Dale equation

$$n(x, y, z) = 1 + K_g \rho(x, y, z) \quad (1)$$

where K_g is the Gladstone-Dale constant that changes depending upon gas species and varies slightly with the light wavelength. In holographic interferometry, double exposure interferograms are generated by exposing the film to the object and the reference beam, respectively. For infinite fringe interferometry, the object beam passes through the flowfield, its

phase changes due to variations of the refractive index caused by density changes between exposures but the phase of the reference beam does not change. The phase shift of the object beam relative to the reference beam between exposures is calculated by integrating

$$\Delta\phi(x_{im}, y_{im}) = \frac{2\pi}{\lambda} K_g \int_0^{L_o} (\rho(x, y, z) - \rho_0) dl \quad (2)$$

where λ is the wavelength of the light, n_0 the refractive index of the undisturbed flow and L_o the length of light path through the test section. The image intensity of the infinite-fringe interferograms I can be calculated by

$$I = 1 + \cos(\Delta\phi(x_{im}, y_{im}) + \phi_0) \quad (3)$$

where (x_{im}, y_{im}) denotes the image plane, and ϕ_0 is an initial phase shift to compensate for any phase shift between two exposures and is taken as zero in most cases. The fringe shift N is given by

$$N = \frac{1}{2\pi} \Delta\phi(x_{im}, y_{im}). \quad (4)$$

This corresponds to the fringe number in infinite-fringe interferograms. One should integrate the density along the actual light path by using Eq.(2) as the light deflects through the flowfield in the test section, but the procedure is computationally expensive. The straight line approximation^[4] is accepted in the present work, which was shown to be a good approximation when the test section is not too big and the density change is not too large. In the case of finite-fringe interferograms achieved by tilting the reference beam between exposures, the image intensity is given by

$$I = 1 + \cos(\Delta\phi(x_{im}, y_{im}) + 2\pi v_x x_{im} + 2\pi v_y y_{im}) \quad (5)$$

where v_x and v_y are the special frequency components of the unperturbed fringes.

Schlieren method is also a very popular flow visualization technique. The intensity of each point in schlieren photographs is proportional to the density gradient perpendicular to the knife edge because the ray deflection is proportional to the density gradient. When the knife is set to be perpendicular to the x -axis in the physical space the intensity I is proportional to the integration of the density gradient along the light ray

$$I \propto \int_0^{L_o} \frac{\partial \rho(x, y, z)}{\partial x} dl \quad (6)$$

Shadowgrams are widely used in aerodynamic experiments, in which the image intensity is proportional to the gradient of the integration of

$\text{grad} \rho(x, y, z)$ in the direction perpendicular to the light ray, which can be calculated by

$$I \propto \text{grad} \int_0^{L_o} \text{grad} \rho(x, y, z) dl \quad (7)$$

Since both the schlieren and shadowgraph methods can provide only qualitative information, these methods are not used as frequently as interferometry in applications to the CFD validation.

3 TWO-DIMENSIONAL CASES: SHOCK WAVE REFLECTION AND DIFFRACTION

We now consider the visualization of two-dimensional fluid flows. The optical setup of experiments is schematically shown in Fig.1. In this setup, the light beam is split into two and collimated with two collimating mirrors: one of these beams is chosen as the reference beam and the other as the object beam. The reference beam and the object beam are then superimposed on a holo-film by means of two reflecting mirrors. In a two-dimensional case, density distributions on planes perpendicular to the light ray within a test section are identical so that Eq.(2) is simply reduced to

$$\Delta\phi(x_{im}, y_{im}) = \frac{2\pi}{\lambda} K_g L_o (\rho(x_{im}, y_{im}) - \rho_0) \quad (8)$$

where the image plane is parallel to the computational plane and L_o is the width of the test section.

The first test case of two-dimensional flow flows is for a shock wave diffracting over a 90° corner at

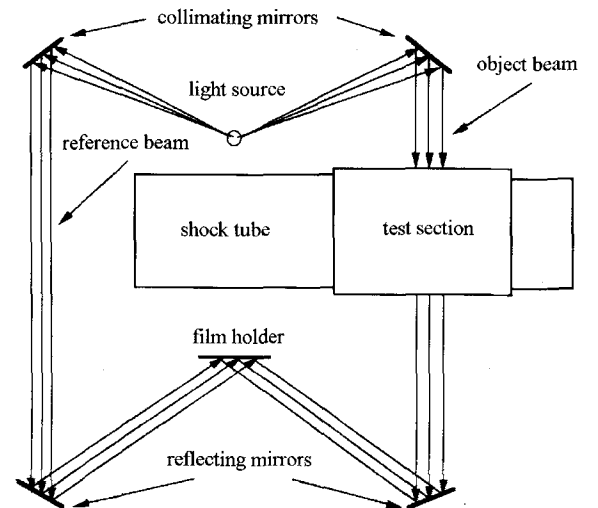


Fig.1 Schematic for constructing two-dimensional interferograms

$M_i = 1.3$, which is numerically simulated by solving the Euler equations with a dispersion-controlled scheme^[20] implemented with non-reflecting boundary conditions described by Jiang et al.^[21]. The efficiency of the scheme has been reconfirmed by Zhuang^[22]. The numerically-determined density is processed to produce a synthetic interferogram by using Eq.(8) and the resulting image is shown in Fig.2, where the transmitting shock diffracts over the corner, expansion waves propagate upstream and the primary vortex develops from the corner. The experimental interferogram obtained by using holographic interferometry is shown in Fig.3. The isopycnics and a schlieren

photograph computed with the same density data by using Eq.(6) are shown in Figs.4 and 5, respectively.

By comparing Fig.2 with Fig.3, it can be observed that in these two photographs the number of fringes is the same, transmitting shocks are identical and fringe distributions coincide with each other. Therefore, a good agreement between them can be concluded. Minor discrepancy exists near the corner and at the rigid wall. The discrepancy can be attributed to the effect of viscosity, that is, the Euler equations are solved for numerical simulations, which require a slip boundary condition, instead of no-slip boundary in experiments. From this comparison, the

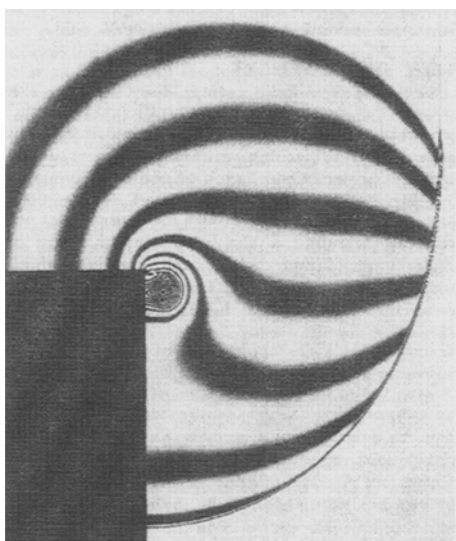


Fig.2 Numerical interferogram of a shock wave diffracting over a 90° corner at $M_i = 1.3$

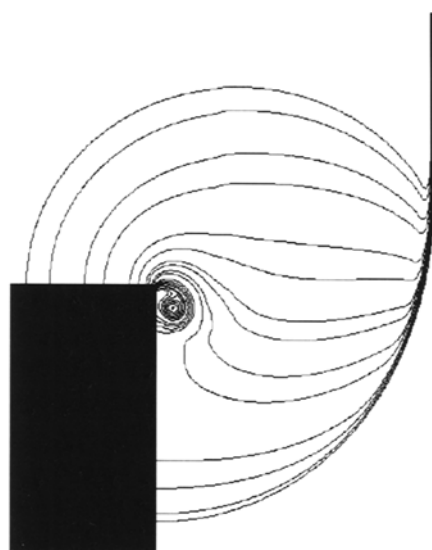


Fig.4 Isopycnics of a shock wave diffracting over a 90° corner at $M_i = 1.3$

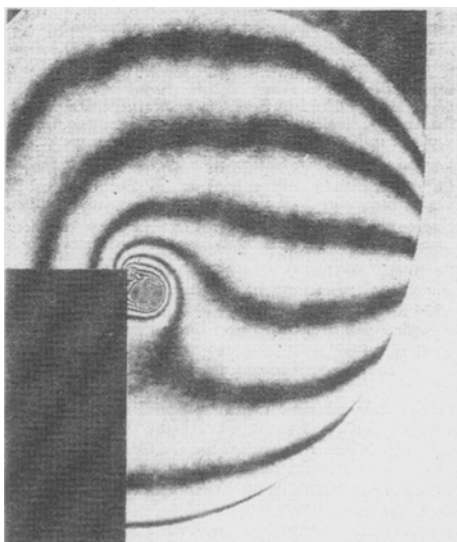


Fig.3 Experimental interferogram of a shock wave diffracting over a 90° corner at $M_i = 1.3$

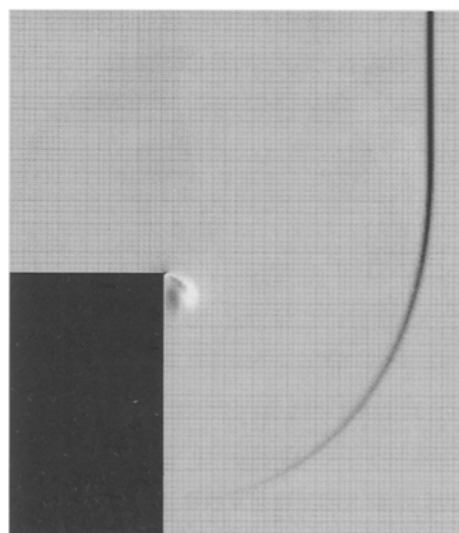


Fig.5 Numerical schlieren of a shock wave diffracting over a 90° corner at $M_i = 1.3$

agreement or the disagreement on wave structures can be decided readily and the factors contributing to the disagreement can be easily deduced. Such a comparison is very important for the shock wave research since wave structures are specially emphasized in this way.

Quantitative validation is also possible in this case by quantifying the experimental interferogram as shown in Fig.3. Since the actual level of the density shift between fringes is known, counting the number of fringes between the locations of known density and the points of interest provides some quantitative density information^[8] for validation. However, the positions of specific isopycnics, as shown in Fig.4, cannot be accurately determined from the experimental interferogram. It is usually assumed that the middle line of each fringe is the position of the corresponding isopycnics. Unfortunately, this will introduce errors because of high non-linearity of the flowfields in many cases of interest. Actually, most validations widely accepted are carried out by comparing Fig.4 with Fig.3, but it is obvious that the comparison between Fig.2 and Fig.3 could gain more credibility of numerical simulations.

Another advanced technique is Fourier transform fringe analysis, which is applied to finite-fringe interferograms to obtain actual density of flowfields with error levels among fractions of the density difference between two neighboring fringes^[15]. However, if the density jump across a shock wave is larger than the density difference between the two fringes, the relevant area of the flowfields is very difficult to be quantified. In the case, a phase-unwrapping algorithm is required to determine the correct fringe shift. However, such an algorithm will not work if the shock waves are everywhere strong^[12], since it requires a starting point where the magnitude of the fringe shift is less than one. In conclusion, these quantifying methods are very useful in practice but will result in the loss of accuracy to a certain extent or be limited to some special cases when trying to extract numerical information out of experimental interferograms. It seems that the present validation mentioned above makes the best use of the experimental data.

Figure 5 shows a schlieren photograph of the shock wave diffraction. Features related to sharp discontinuities in density, such as the shock waves and the slip line, are easily visualized against the background but continuous density distributions are poorly visualized. Shadowgrams also show the similar characters in the flowfield. Therefore, for a quantitative validation of numerical solutions, the interfero-

gram is preferable.

Figure 6 presents a special interferogram of a shock wave focusing after its reflection from a parabolic reflector, that is, a planar shock wave at $M_i = 1.6$ propagates toward the reflector, and reflects back, and then the reflected shock wave focuses at the focal point of the reflector. A quantitative validation can be explained with this figure that consists of two parts: the experimental image in the left and the numerical one in the right. If the relevant fringes in both results match with each other exactly, the agreement can indicate that the numerical result is the same as the experimental data. If there are some discrepancies in the position of each pair of the relevant fringes, the accuracy of the numerical result can be evaluated from the discrepancies. For instance, the maximum shift in positions of the relevant fringe in Fig.6 is less than 30% of the interval between neighboring fringes. Considering that one fringe shift represents a density change of 10% of the initial density in front of the planar shock wave, one can conclude that this maximum discrepancy indicates that the maximum error in density is less than 3.0% of the initial density according to fringe pattern analysis. This implies that the accuracy level reached could be as high as one obtained by quantifying the experimental interferogram with Fourier transform fringe analysis. Moreover, the accuracy level discussed is at the extreme position, the actual level is much higher in the most area of the flowfield. However, there may be something uncertain in the experiment when one evaluates the accuracy level of numerical results according to experimental data, but its discussion is out of the scope of this paper.

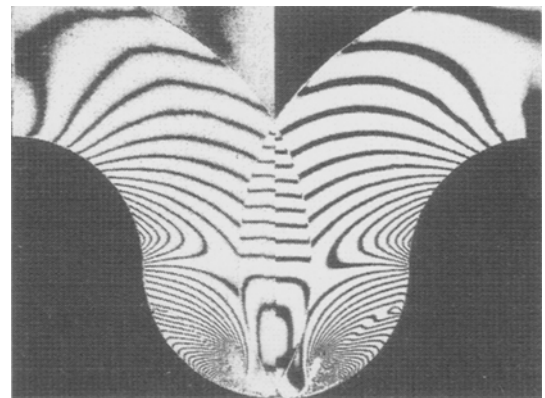


Fig.6 Interferogram of a shock wave focusing after its reflection from a parabolic reflector to demonstrate quantitative validation: experimental result (the left) and numerical one (the right)

4 AXISYMMETRICAL CASES: SHOCK WAVE PROPAGATIONS

In the case of axisymmetric fluid flows, the principle for constructing interferograms is schematically shown in Fig.7. Here the reference beam and the object beam are still superimposed on the holo-film but the density distribution on the planes perpendicular to the light ray within the test section varies along the light path. Considering this difference and the symmetry of the physical domain, when the light path is perpendicular to the axis of symmetry, the phase shift expressed by Eq.(2) can be calculated by the following equation

$$\Delta\phi(x_{im}, y_{im}) = \frac{4\pi}{\lambda} K_g \int_{y_{im}}^R (\rho(x, r) - \rho_0) dr \quad (9)$$

where R is the diameter of the physical domain and the integration is carried out from $r = y_{im}$ to R along the light path. This integration is not as straightforward as in two-dimensional cases but still quite simple to calculate. More detailed description of the density integration was given by Havener et al.^[3].

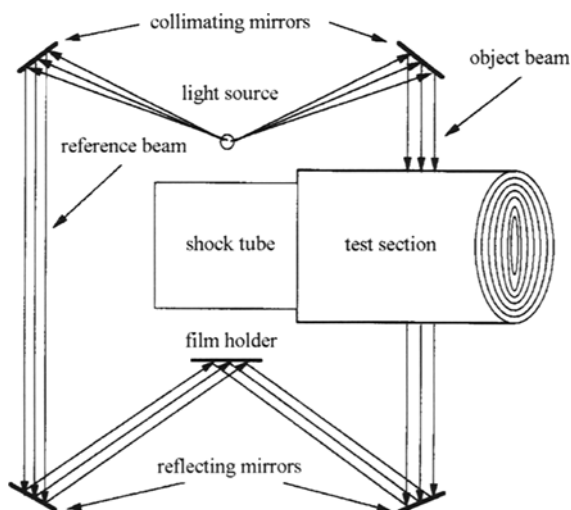


Fig.7 Schematic for constructing axisymmetrical interferograms

As the first axisymmetric case, a shock wave propagating in a tube with a sudden area change in its cross section, referred to as an expansion tube (a large diameter chamber is connected to a small diameter shock tube), is simulated by using the same numerical code as used in two-dimensional cases. The Mach number is taken to be $M_i = 1.3$ and the diameter ratio, the large chamber to the shock tube, is taken as 2 : 1. In the experiment, this large chamber is specially designed to have an aspheric cross section which allows the collimated incident ray to traverse

the transparent wall of the test section parallelly, and to emerge parallelly. The detailed description of the experiment was given by Takayama et al.^[23] and Jiang et al.^[16]. An experimental interferogram of the flow-field is shown in Fig.8, the corresponding numerical one is presented in Fig.9 and the isopycnics of the numerical solutions in the symmetric plane are plotted in Fig.10.

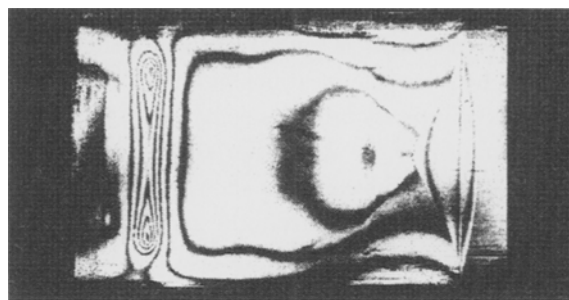


Fig.8 Experimental interferogram of a shock wave propagating in an expansion tube at $M_i = 1.3$

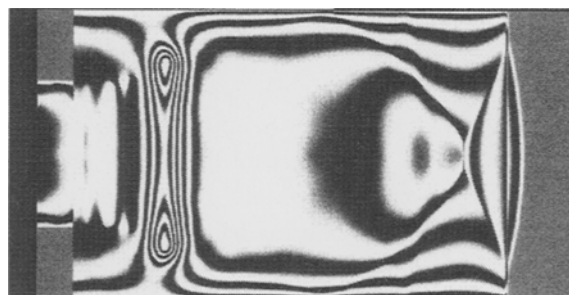


Fig.9 Numerical interferogram of a shock wave propagating in an expansion tube at $M_i = 1.3$

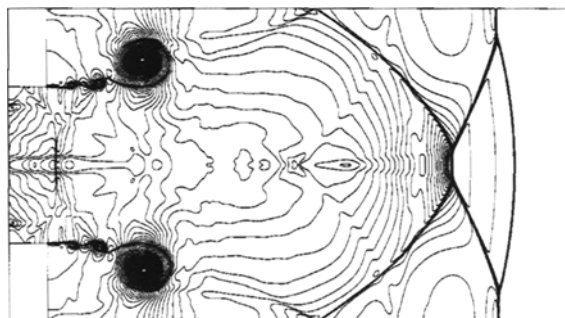


Fig.10 Numerical isopycnics of a shock wave propagating in an expansion tube at $M_i = 1.3$

As is expected, the difference between the interferogram shown in Fig.8 and the numerical isopycnics in Fig.10 is obvious because of the axisymmetric density distribution. The transmitting shock wave, the

primary vortex ring and the shear layer appear in different ways in these two kinds of the displays. Furthermore, the shock wave reflection from the tube wall is clearly visible in the isopycnics, but smeared in the interferogram due to effects of the integral view of the whole density field. Hence the physical understanding of the wave phenomena is not so easy to reach and conclusions about the CFD validation are difficult to draw. However, if the validation strategy is changed by constructing a numerical interferogram as shown in Fig.9 and comparing it with the corresponding experimental one in Fig.8, it is readily observed that the agreement between the numerical and the experimental interferograms is excellent. This indicates that an acceptable comparison between numerical and experimental results can be achieved only when two results are presented based on the same principle. Under such circumstances, we can reach a conclusion much easier and avoid any mis-interpretation.

The second axisymmetric case presented is for the diffraction of a shock wave discharging from a shock tube into air at a shock Mach number of $M_i = 1.6$. Its computational domain is similar to the first case but without that big diameter tube. The numerical result is given in Fig.11 and the experimental interferogram is shown in Fig.12. It can be seen from the comparison that the agreement between the computational result and the experimental data is excellent. This is not only because the number of fringes is identical but the distribution of the individual fringes matches well with each other with only minor exceptions. In fact, the largest deviation in fringe positions is less than half of the fringe distance. This case is more useful since there are many fringes that can be utilized in validation.

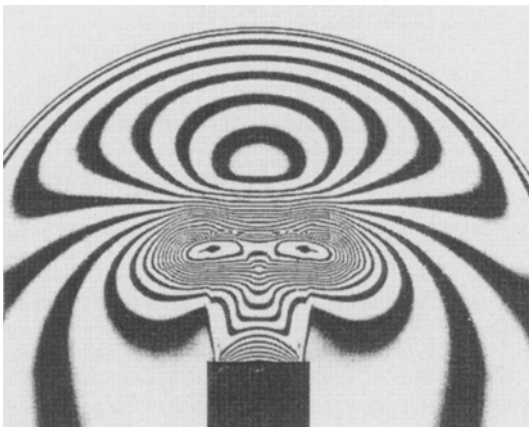


Fig.11 Numerical interferogram of a shock wave discharging from a shock tube at $M_i = 1.6$

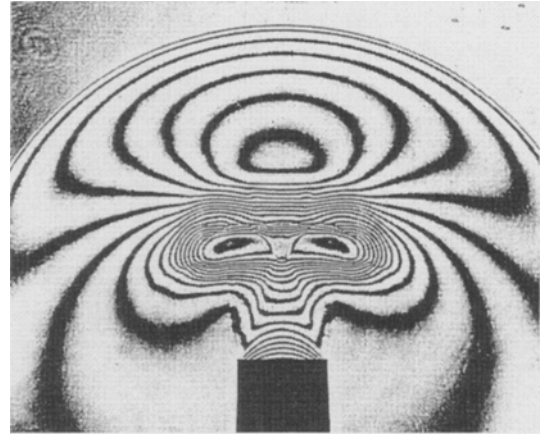


Fig.12 Experimental interferogram of a shock wave discharging from a shock tube at $M_i = 1.6$

It is also necessary to point out that perturbations in the test section may make experimental fringes move slightly forwards or backwards so that the experimental uncertainty could impose some difficulties on estimating the accuracy of numerical solutions. Moreover, the difficulty in timing numerical results to match exactly with experiments also results in fringe shift in the numerical image. These facts have to be considered to achieve a reliable validation.

Figure 13 shows a special interferogram of a shock wave propagating from a shock tube into an expansion tube at $M_i = 2.0$, where the experiment photo (upper half) and the numerical result (lower half) are combined together. Further validation can be explained by this figure, as discussed about Fig.6 in the last section. The maximum shift in fringe positions observed from Fig.13 is less than 20% of the interval between two neighboring fringes. Because one fringe shift represents a density change of 13.68% of the initial density in front of the shock wave, this maximum discrepancy means that the maximum error in density is less than 2.8% of the initial density according to fringe pattern analysis. However, it must be



Fig.13 A special interferogram of a shock wave propagating from a shock tube into an expansion tube at $M_i = 2.0$: the experiment photo (upper half) and the numerical result (lower half)

pointed out that the maximum discrepancy is not in the density distribution in the axisymmetric plane, but in the integrated density along the light path within the test section.

In addition, the reliability of the validation also depends on the purpose of study. For example, if the shock wave motion and shock wave interaction are emphasized in this case, the agreement concluded from the comparison is excellent. However, if shock-wave/boundary-layer interaction is to be investigated, it is obvious that the validation is not acceptable because the boundary layer is not visible in the experimental results due to experimental limitations and the numerical solutions are only based on the Euler equations.

Quantification of the axisymmetric interferogram shown in Fig.12 is also possible by performing an inverse transformation of the integrated image data to obtain the density information on the symmetric plane. However, the computational process may break down and the accuracy of the numerical value may be compromised in the case of flowfields with many strong shock waves. We, therefore, conclude that the present validation for the axisymmetric case is more efficient and easier to carry out.

5 THREE-DIMENSIONAL CASE: SHOCK WAVE DIFFRACTION

For three-dimensional flowfields, the reconstruction of density from interferograms is, at least, theoretically possible with the use of tomographic techniques which allows an unknown density distribution to be determined from line integrals of density through the whole distribution. However, in order to perform the inversion successfully, tens of interferograms in different viewing directions at the same time must be provided for the reconstruction of complex flowfields^[13,14]. As can be imagined, the tomographic inversion is immensely difficult in highly unsteady flows because it is almost impossible to record many flow images simultaneously. In comparison, creating computational interferograms from the three-dimensional density distribution is more feasible for CFD validation.

A schematic for integrating the three-dimensional density with the previously-used method^[4] is shown in Fig.14, where the interval $x_j \leq x_{j+1}$ defines the intersection of the light path with a computational cell. Tracing the light path as it passes through the flowfield and integrating the appropriate function of the refractive index along

this path are computationally expensive even if the straight line approximation is adopted. In this process, it is necessary to determine the computational cell that the light intersects with, find the intersected points on the computational cell, interpolate the density at these two points, calculate the integral for this segment and add it to the appropriate sum. The first three operations are the most time-consuming for the density integration. To overcome this difficulty and make the three-dimensional post-processing more efficient, a fast algorithm is proposed by Jiang et al.^[5]. As a result of the improvement, the newly developed code is about 20 times faster than the one based on the conventional integrating algorithm.

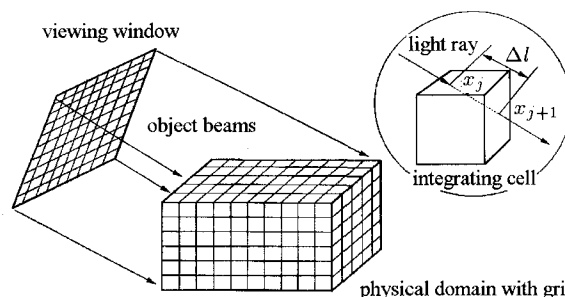
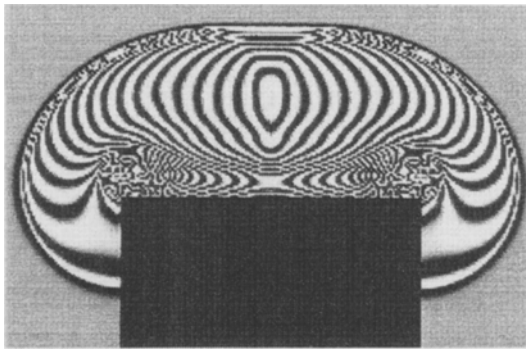


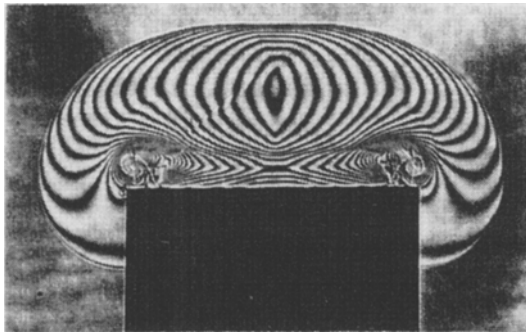
Fig.14 Schematic of three-dimensional density integration

The three-dimensional test case is a shock wave diffraction, created by discharging a transmitting shock wave from the open-end of a square shock tube into ambient air at a Mach number of 1.5. The shock wave at the open-end is initially planar, but quickly develops into a spherical shape via a three-dimensional transition with time.

The three-dimensional hyperbolic system of the conservation laws for a perfect gas was solved using a dispersion-controlled scheme^[20] on an equally-spaced grid with $200 \times 150 \times 150$ mesh points. Experiments were conducted in a $40 \text{ mm} \times 40 \text{ mm}$ square cross-sectional tube connected to a $60 \text{ mm} \times 150 \text{ mm}$ diaphragmless shock tube in the Shock Wave Research Center, Tohoku University, Japan^[24]. The diffraction of the shock wave was visualized with the double exposure holographic interferometry. Both numerical and experimental results viewed in three viewing directions were given in Figs.15 through 17, respectively. Figure 15 shows the side view of the shock wave diffraction, which is in a view direction normal to the side-wall of the shock tube. Figure 16 shows the corner view that is observed along the diagonal line of the square cross section. Figure 17 shows the axial view from the direction of 15° degree off the axis of symmetry.

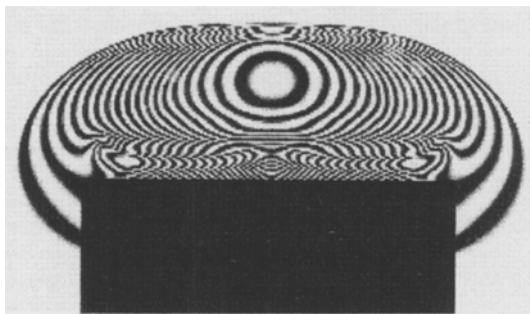


(a) Numerical interferogram

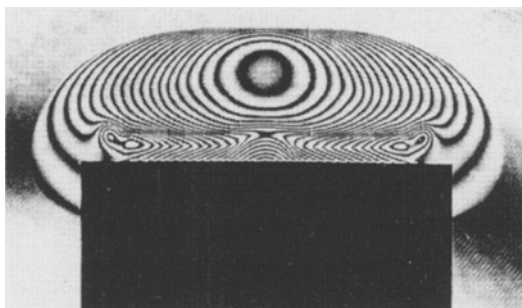


(b) Experimental interferogram

Fig.15 Side views of a three-dimensional shock wave diffracting from a square shock tube at $M_i = 1.5$

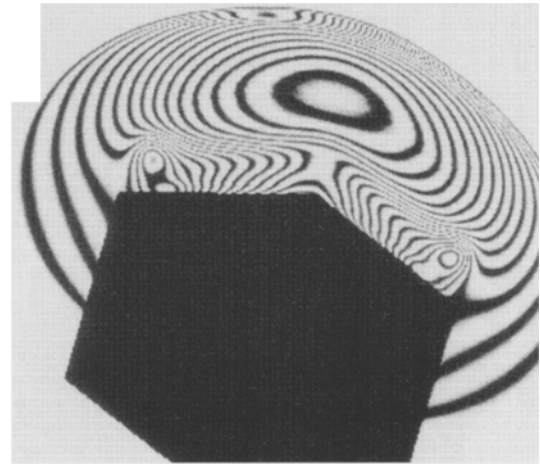


(a) Numerical interferogram

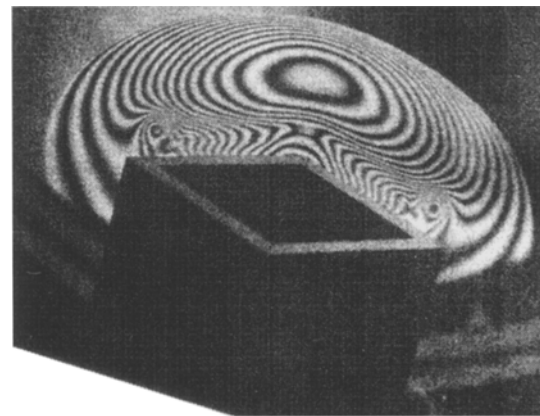


(b) Experimental interferogram

Fig.16 Corner views of a three-dimensional shock wave diffracting from a square shock tube at $M_i = 1.5$



(a) Numerical interferogram



(b) Experimental interferogram

Fig.17 Axial views of a three-dimensional shock wave diffracting from a square shock tube at $M_i = 1.5$

Carefully examining each pairs of interferograms shown in Fig.15 through Fig.17, it is seen that the agreement between the numerical and experimental results is good: the number of fringes and their distributions coincide very well with each other. The only discrepancy observable between the numerical and experimental interferograms is near the exit in Figs.15(a) and 16(a) due to the fact that the resolution for displaying these numerical images is not fine enough to distinguish as many fringes as shown in the experimental interferograms in Figs.15(b) and 16(b), where density gradients are very high. Three pixels, at least, are necessary to visualize one fringe: a dark pixel between two white pixels. If the space between two fringes is smaller than one pixel, computed fringes will be displayed incorrectly. This problem can be avoided when a numerical image is created with fewer fringes, for example, see the images shown in Fig.17. Apart from this minor discrepancy, all the wave phenomena, such as the non-uniform flow expansion

created at corners and a secondary shock wave developed near the primary vortex loop, appear to be identical in numerical and experimental results. From the comparison of these results obtained by viewing from three viewing directions, it can be concluded that the numerical solutions are well validated.

It is obvious that for the validation of numerical simulations of such a complex flowfield, a check on numerical solutions with only a limited set of point measurements in the flowfield is not sufficient and a comparison between topological flow structures from both numerical and experimental results must be made.

Comparing Figs.15 and 16 with Fig.18 reveals some differences between interferometric fringes and numerical isopycnics in both the mid-wall symmetrical plane and the diagonal plane. Because the fringes in Figs.15 and 16 represent the integrated density seen by the individual light ray passing through a test section, many planes having different density distributions overlap. This results in many fringes in the central area in the interferograms as shown in Figs.15 and 16 but there are no density changes there, as shown in Fig.18. Moreover, from numerical isopycnics shown in Fig.18(b), the secondary shock wave is clearly observable but it is not easily identified from the interferograms shown in Fig.16. According to the above discussion, it is understood that, for a three-

dimensional flow visualization, some physical features may appear to be smeared and some non-physical features may be created. Therefore, the experimental data needs to be carefully interpreted with reliable numerical results that are capable of showing three-dimensional transient phenomena in detail.

As is well known, both the Computational Fluid Dynamics and the experimental flow visualization are important tools in the research of fluid science. Because the most interesting problems in engineering are three-dimensional and transient, and contain many complex flow phenomena, investigations into such flowfields are very useful and important. However, it can be very difficult. It may be too hard to expect the experimental flow visualization to provide all the necessary information for understanding these complex flowfields. However, the present study shows that it may be possible to circumvent this difficulty through the interferometry that can provide interferograms clear enough to validate numerical solutions. In other words, experimental images of a three-dimensional flowfield only need to provide information for validation of numerical solutions. The numerical results thus validated, in return, provide some useful information for interpreting the complex interferometric patterns. As a result, such a CFD validation works as a tool that combines the CFD and the experiment together for exploration of the flow physics that can never be done with the CFD or the experiment alone.

6 CONCLUSIONS

Computational simulation of the optical flow visualization can create a direct comparison between numerical and experimental results, which is demonstrated to be a promising way to approach the reliable validation of numerical solutions, especially for three-dimensional complex flowfields where quantification of experimental interferograms is almost impossible. This comparison with quantitative characters is an effective approach to the whole flowfield validation without any loss of accuracy on both experimental data and numerical results. However, in order to achieve reliable validation, the flowfield of interest must be represented correctly by the selected physical models, visualized clearly by interferometry and displayed properly by computer facilities. In addition, fringe patterns of experimental results in axisymmetric and three-dimensional flowfields need to be carefully interpreted by taking into account density-integrated effects.

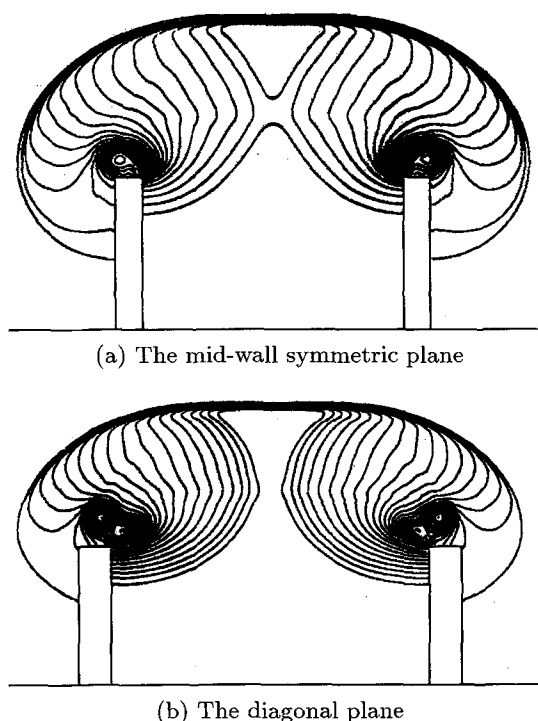


Fig.18 Isopycnics in two symmetric planes of a three-dimensional shock wave diffracting from a square shock tube at $M_i = 1.5$

REFERENCES

- 1 Babinsky H, Meguro T, Jiang Z, et al. Numerical visualization of shock wave flow in an expanding tube and comparison with experiment. In: Khalighi et al. eds. *Exp and Numerical Flow Visualization*, Vol 218, ASME, Hilton Head, South Carolina, 1995. 89~94
- 2 Babinsky H, Takayama K. CFD validation strategies for compressible flow using interferometry. *AIAA 96-0438*, 1996
- 3 Havener AG, Obergefell LA. Computational interferometric description of nested flow fields. *Optical Engineering*, 1985, 24: 441~445
- 4 Yates LA. Images constructed from computed flow-field. *AIAA Journal*, 1993, 31: 1877~1884
- 5 Jiang Z, Takayama K. An investigation into the validation of numerical solutions of complex flowfields. *J Computational Physics*, 1999, 151: 479~497
- 6 Inoue O, Takahashi M, Takayama K. Shock wave focusing in a log-spiral dust. *AIAA Journal*, 1993, 31: 1150~1155
- 7 Sasoh A, Takayama K, Saito T. A weak shock wave reflection over wedges. *Shock Waves*, 1992, 2: 277~283
- 8 Sun M, Takayama K. A holographic interferometric study of shock wave focusing in a circular reflector. *Shock Waves*, 1996, 6: 323~336
- 9 Takayama K, Jiang Z. Shock wave reflection over wedges: a benchmark test for CFD and experiments. *Shock Waves*, 1997, 7: 191~203
- 10 Jiang Z, Liu J, Ni G, et al. The calculation of the density field from axisymmetric schlieren interferograms by the image processing techniques. *Acta Mechanica Sinica*, 1993, 9: 22~26
- 11 Sharma SP, Ruffin S. Density measurements in an expanding flow using holographic interferometry. *AIAA 92-0809*, 1992
- 12 Bone DJ. Fourier fringe analysis: the two-dimensional phase unwrapping problem. *Applied Optics*, 1991, 30: 3627~3632
- 13 Parker SCJ. The quantitative analysis of transonic flows by holographic interferometry. [PhD Thesis], University of Warwick, UK, 1993
- 14 Morton JW, Houwing AFP, Boyce RR, et al. Tomographic reconstruction of jet and shock layer flows. In: Houwing et al eds. *Proc of the 21st Int Symp on Shock Waves*, Vol 1, Great Keppel Island, Australia, July 20~25, 1987. 435~441
- 15 Takeda M, Ina H, Kobayashi S. Fourier transform method of fringe-pattern analysis for computer-based tomography and interferometry. *J Optics Soc Am*, 1981, 22: 824~831
- 16 Jiang Z, Takayama K, Babinsky H, et al. Transient shock wave flows in tubes with a sudden change in cross section. *Shock Waves*, 1997, 7: 151~162
- 17 Jiang Z, Onodera O, Takayama K. Three-dimensional reflection of shock waves propagating in square cross-sectional tubes. In: Houwing et al. eds. *Proc of the 21st Int Symp on Shock Waves*, Vol 2, Great Keppel Island, Australia, July 20~25, 1987. 1499~1501
- 18 Tam TC, Brock NJ, Cavolowsky JL, et al. Interferometry at the NASA-Ames hypervelocity free-flight aerodynamic facility. *AIAA 91-0568*, 1991
- 19 Tamura Y, Fujii K. Visualization for computational fluid dynamics and the comparison with experiments. *AIAA 90-3031*, 1990
- 20 Jiang Z, Takayama K, Chen YS. Dispersion conditions for non-oscillatory shock capturing schemes and its applications. *Comp Fluid Dynamics J*, 1995, 2: 137~150
- 21 Jiang Z, Chen YS, Kuwahara K. Approximate non-reflecting inflow-outflow boundary conditions for calculations of Navier-Stokes equations for internal flows. *Acta Mechanica Sinica*, 1993, 9: 289~297
- 22 Zhuang FG. On numerical techniques in CFD. *Acta Mechanica Sinica*, 2000, 16: 193~216
- 23 Takayama K, Onodera O. Shock wave propagation past circular cross sectional 90° bends. In: Archer, Milton eds. *Proc of the 14th Int Symp on Shock Tubes and Shock Waves*, University of Sydney, New South Wales, Australia, 1983. 205~211
- 24 Abe A. Shock waves discharged from the open end of shock tubes. [Doctoral Thesis], Graduate School of Tohoku University, Sendai, Japan, 1991